Fuel 306 (2021) 121616

Contents lists available at ScienceDirect

Fuel

journal homepage: www.elsevier.com/locate/fuel

Full Length Article

Pyrolysis of bio-derived dioxolane fuels: A ReaxFF molecular dynamics study

Hyunguk Kwon [a], Yuan Xuan [b,*]

[a] Department of Chemical Engineering, The Pennsylvania State University, University Park, PA, 16802, USA
[b] Department of Mechanical Engineering, The Pennsylvania State University, University Park, PA, 16802, USA

ARTICLE INFO

Keywords:
Molecular dynamics
ReaxFF
Pyrolysis
Dioxolane
Biodiesel

ABSTRACT

Alkyl-substituted 1,3-dioxolanes, including 4,5-dimethyl-2-pentan-3-yl-1,3-dioxolane (Fuel 1), 4,5-dimethyl-2-pentyl-1,3-dioxolane (Fuel 2), and 2-(heptan-3-yl)-4,5-dimethyl-1,3-dioxolane (Fuel 3), have been recently suggested as potential biodiesels. In this paper, we investigate the initial pyrolysis of the alkyl-substituted 1,3-dioxolanes at high temperatures using ReaxFF molecular dynamics (MD) simulations. We analyze the decomposition rate, reaction mechanism, and product distribution in the pyrolysis of the three alkyl 1,3-dioxlanes. The three fuels primarily decompose to 4,5-dimethyl-1,3-dioxolane radical and hydrocarbons derived from the alkyl side-chains. The further decomposition of 4,5-dimethyl-1,3-dioxolane radical primarily leads to 2-C_4H_8 and CO_2 within a few decomposition steps. The hydrocarbon product distribution is significantly affected by the molecular structure of the alkyl side-chain, which would have a strong influence on the sooting tendency of these fuels. The ReaxFF simulations predict that the order of sooting tendency would be Fuel 3 > Fuel 1 > Fuel 2, which agrees with the measured sooting tendency trend. Based on the pyrolysis mechanism identified by ReaxFF, we propose a new alkyl dioxolane, 4-hexyl-5-methyl-1,3-dioxolane (Fuel 4), which might produce even less soot, by modifying the molecular structure of Fuel 2. Our ReaxFF simulation shows that Fuel 4 produce much less C_4H_8, an effective non-aromatic soot precursor, than Fuel 2. Moreover, more carbon atoms are bonded to each oxygen atom in Fuel 4 than Fuel 2, which would help reduce soot yield by removing more carbon atoms from the soot-producing pool of species. The major decomposition pathways identified in this work can be used to develop chemical kinetic models for 1,3-dioxolane based compounds, as biodiesel components, applicable to combustion engine simulations. We also demonstrate that the chemical kinetic insight offered by ReaxFF simulations can be used to design new fuel molecules with more desired properties.

1. Introduction

Biomass is the only sustainable source of organic compounds [1]. Therefore, there have been a lot of efforts on the development of new technologies to convert non-food biomass feedstocks into biofuels [2]. Biofuels can be used in energy conversion processes with different purposes, including road transport, aviation, and electricity generation [3]. The use of biofuels offers a significant benefit in reducing greenhouse gas and particulate matter (PM) emissions compared to traditional fuels [4]. However, there are still drawbacks that restrict the extensive application of biofuels, including the shortage of feedstock supply, relatively low energy contents, compatibility issues with existing petroleum-based infrastructures, and poor cost competitiveness [5]. To resolve these issues, significant efforts have been made to produce advanced biofuels.

Compounds containing 1,3-dioxolane, a five-membered heterocyclic acetal with two oxygen atoms at the 1, 3-positions (see Fig. 1(a)), have received attention as renewable gasoline or diesel blendstocks. For example, Harvey *et al.* introduced dioxolane mixtures (2-ethyl-2,4,5-trimethyl-1,3 dioxolane and isomers) formed from renewable 2,3-butanediol as a sustainable gasoline blending component or diesel oxygenate [6]. The dioxolane mixtures show an anti-knock index (90.5) comparable to high octane gasoline, and net heat of combustion 34 % higher than ethanol. Harrison *et al.* synthesized three substituted 1,3-dioxolane compounds by acid catalyzed condensation of bio-derived diols containing two hydroxyl groups [7]. The fuels exhibit comparable net heat of combustion to conventional biodiesels, but significantly higher cetane numbers and lower melting points. Staples *et al.* proposed a solvent-free

* Corresponding author.
E-mail address: yux19@psu.edu (Y. Xuan).

https://doi.org/10.1016/j.fuel.2021.121616
Received 29 April 2021; Received in revised form 26 July 2021; Accepted 31 July 2021
Available online 11 August 2021
0016-2361/© 2021 Elsevier Ltd. All rights reserved.

method for producing five alkyl-substituted dioxolane fuels from bio-derived aldehydes [8]. Compared to petroleum diesel, the suggested 1,3-dioxolane fuels show an increased cetane number, as well as decreased viscosity, freezing point and soot production, which indicates that the use of the dioxolane compounds as blendstocks would be potentially beneficial.

One important task for the use of 1,3-dioxolane based fuels is to identify the complex reaction networks during their pyrolysis and combustion with quantified reaction rates. The identified reaction mechanisms can be potentially used to predict important combustion characteristics, such as ignition, extinction, heat release, and formation of pollutants. Previous studies have investigated the reaction kinetics of 1,3-dioxolane in pyrolysis [9,10], photolysis [11–13], and radical-involved decomposition [11,14–17]. However, very little has been reported on the reaction kinetics of alkyl-substituted 1,3-dioxolane fuels. Rosas *et al.* investigated the kinetics of thermal decomposition of a series of 1,3-dioxolane based compounds, such as 2-methyl-1,3-dioxolane, 2,2-dimethyl-1,3-dioxolane, and cyclopentanone ethylene ketal, through combined experiments and density functional theory (DFT) calculations [18]. The dioxolanes were found to initially decompose through a concerted four-centered cyclic mechanism to produce acetaldehyde and the corresponding ketone. Other than this study, to the best of our knowledge, the decomposition kinetics for other alkyl-substituted 1,3-dioxolane has not been reported.

The purpose of this study is to investigate the high-temperature pyrolysis of three alkyl 1,3-dioxolanes recently synthesized by Staples *et al.* [8] using ReaxFF-based molecular dynamics (MD) simulation. These fuels are 4,5-dimethyl-2-pentan-3-yl-1,3-dioxolane (Fuel 1), 4,5-dimethyl-2-pentyl-1,3-dioxolane (Fuel 2), and 2-(heptan-3-yl)-4,5-dimethyl-1,3-dioxolane (Fuel 3), and their molecular structures are shown in Fig. 1. Staples *et al.* synthesized five dioxolane fuels [8], however, two of them are excluded in this work. 4,5-dimethyl-2-propyl-1,3-dioxolane is excluded because of its low cetane number (37) that does not meet the diesel standards. This work also does not include 4,5-dimethyl-2-heptyl-1,3-dioxolane, because of its structural similarity to Fuel 2 (with the pentyl side-chain of Fuel 2 replaced by a heptyl side-chain). In this work, we report the decomposition rates and reaction mechanisms of the three alkyl-substituted 1,3-dioxolane fuels during pyrolysis at high temperatures. Product spectrum is also analyzed to estimate their relative sooting tendencies. In addition, based on our simulation results, we propose a new dioxolane fuel that could potentially lead to even lower soot production compared to Fuels 1–3 with similar carbon number. We believe that the results reported in this work provide key chemical kinetic insights on the pyrolysis of alkyl 1,3-dioxolanes as bio-diesel fuels.

2. Simulation details

2.1. ReaxFF method

The ReaxFF is a bond order-dependent force field that can simulate bond formation and bond breaking [19–21]. The bond order is calculated from interatomic distance using an empirical formula that contains the single, double, and triple bond order contributions and is updated at every iteration. The non-bonded interactions, such as van der Waals and Coulomb, are calculated between all atom pairs and they are independent from the bonded-interactions. The electronegative equalization method (EEM), a geometry-dependent charge calculation scheme, is used to calculate the polarization for charges within molecules [22]. The details of the EEM method can be found in Section S1 of the supplementary material. In the ReaxFF method, the energy of the system is partitioned into various contributions and calculated using the following equation,

$$E_{system} = E_{bond} + E_{over} + E_{under} + E_{lp} + E_{val} + E_{tor} + E_{vdWaals} + E_{Coulomb} \quad (1)$$

In the above equation, E_{bond} (bond energy), E_{over} (over-coordination penalty energy), E_{under} (under-coordination penalty energy), E_{lp} (lone pair energy), E_{val} (valence angle energy), E_{tor} (torsion angle energy) are bond-order dependent terms. E_{vdWaals} (van der Waals energy) and E_{Coulomb} (Coulomb energy) are non-bonded terms. The more detailed description can be found in the prior ReaxFF-related papers [19–21]. The current MD simulations were performed within the ReaxFF program implemented in the Amsterdam Density Functional (ADF) software [23].

The first version of ReaxFF for pyrolysis and combustion (CHO-2008) was developed by Chenoweth *et al.* [20]. The force field has been extensively used to study pyrolysis and combustion of hydrocarbons, such as *n*-heptane [24], *n*-dodecane [25], toluene [26], 1,6-dicyclopropane-2,4-hexyne [27], and JP-10 [20]. Recently, a new version of the force field (CHO-2016) was developed by Ashraf *et al.* [28] to improve upon the C1 chemistry. The CHO-2016 force field has shown good capability to describe the pyrolysis and the combustion of single component fuels [28–31] or fuel mixtures [31–33]. All the simulations reported in this paper were performed using the CHO-2016 force field.

2.2. ReaxFF MD simulations

We followed a well-established simulation framework for pyrolysis study using ReaxFF [20,28,31,34]. For each fuel, 40 fuel molecules were randomly placed in a periodic simulation box using an in-house code, where the minimum allowed distance between fuel molecules was set to be 2.50 Å. The size of the cubic box was determined to produce a density of 0.1 kg/dm^3, which corresponds to the initial (ideal gas) pressures from 86 atm (at 1800 K) to 114 atm (at 2400 K) for the systems with Fuel 1 and Fuel 2 and from 74 atm (at 1800 K) to 98 atm (at 2400 K) for the system with Fuel 3. Previously, ReaxFF papers [20,28,31,34] predicted the Arrhenius parameters for pyrolysis of various fuel molecules reasonably well with the number of molecules and density conditions similar to those selected in this work. Snapshots of the simulation initial configuration are shown in Fig. 2 for each fuel. The prepared system was equilibrated through NVT-MD simulation at 1500 K. The NVT-MD simulation indicates that the number of atoms (N), volume (V), and temperature (T) are kept constant during the simulations. The temperature for equilibrium was chosen such that no thermal decomposition happens during the equilibrium simulation. The Berendsen thermostat [35] with a temperature damping constant of 100 fs was used to control the temperature. After the equilibrium simulation, NVT-MD simulations were performed at 1800 K, 2000 K, 2200 K, and 2400 K using a time-step of 0.1 fs. The temperature conditions were selected to represent the

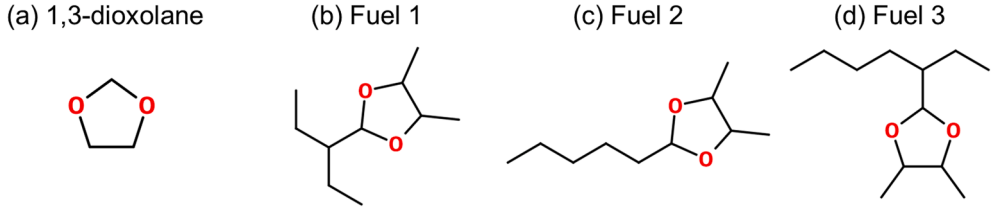


Fig 1. Molecular structure of the dioxolane fuels considered in this work. (a) 1,3-dioxolane ($C_3H_6O_2$), (b) Fuel 1; 4,5-dimethyl-2-pentan-3-yl-1,3-dioxolane ($C_{10}H_{20}O_2$), (c) Fuel 2; $C_{10}H_{20}O_2$, 4,5-dimethyl-2-pentyl-1,3-dioxolane ($C_{10}H_{20}O_2$), and (d) Fuel 3; 2-(heptan-3-yl)-4,5-dimethyl-1,3-dioxolane ($C_{12}H_{24}O_2$).

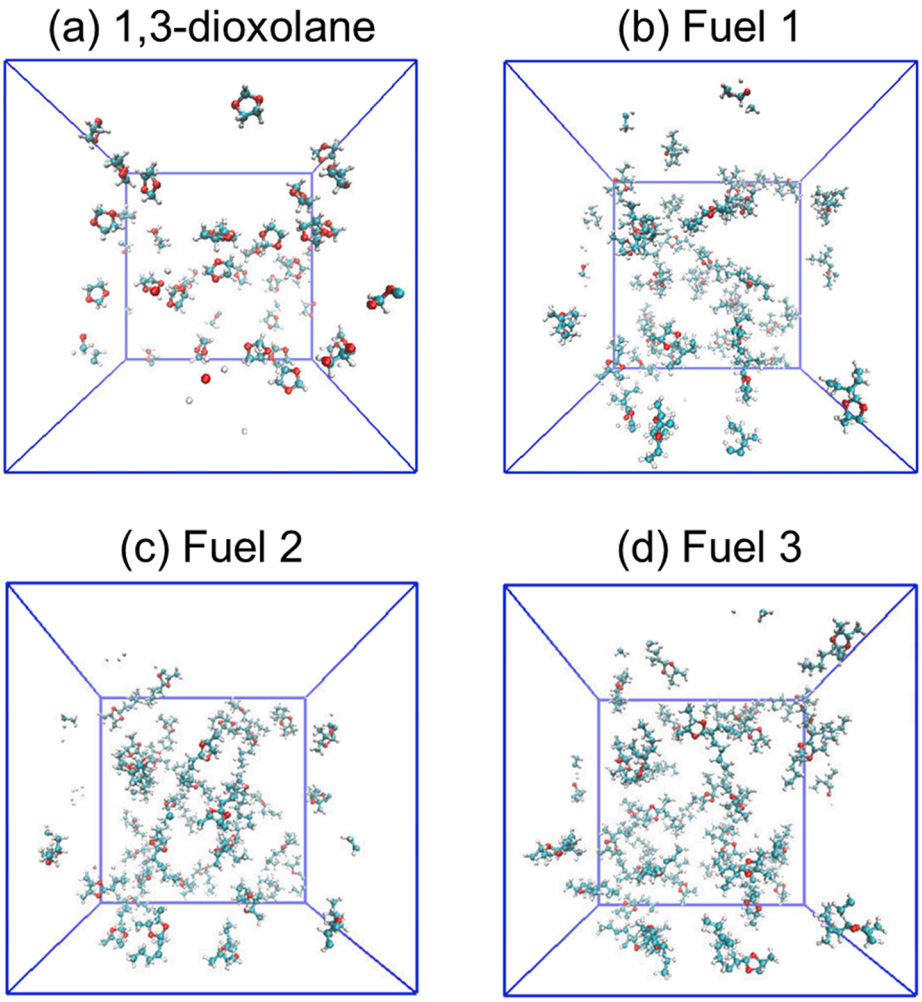


Fig 2. Snapshots of simulation initial configuration for (a) 1,3-dioxolane, (b) Fuel 1, (c), Fuel 2, and (d) Fuel 3 pyrolysis with a density of 0.1 kg/dm^3. The cyan, white, and red spheres indicate carbon, hydrogen, and oxygen atoms, respectively. (For interpretation of the references to colour in this figure legend, the reader is referred to the web version of this article.)

pyrolysis temperature of fuels in laboratory-scale flames and gasoline or diesel combustion engines. Our previous ReaxFF work showed that the time step (0.1 fs) is small enough to provide the appropriate temporal resolution under the temperature conditions of the current study [34]. The simulations were performed with 10 independent starting configurations at a given temperature, and the results were ensemble-averaged to get statistically meaningful results.

The reaction events were identified using an in-house reaction analysis code. A reaction was considered to occur when species with different chemical formula were identified between two consecutive simulation steps. The reactions were identified in each NVT-MD simulation. Then, the reaction occurrences were averaged over the 10 independent simulations at each temperature. The same process has been successfully used to identify reactions in our previous studies [34,36]. The source code of the reaction analysis tool using ReaxFF results is made publicly available at https://github.com/hukwon/ReaxFF_reaction_analysis.

3. Results and discussions

3.1. Pyrolysis of 1,3-dioxolane

In this section, reaction rate constant and product spectrum during the pyrolysis of 1,3-dioxolane (Fig. 1(a)) are investigated using ReaxFF simulations. They are compared with literature data to demonstrate that our ReaxFF-based MD simulations are capable of capturing the 1,3-dioxolane chemistry.

The global fuel decomposition rate constant (k) at each temperature is determined using the integrated first-order rate law equation,

$$\ln(N_0) - \ln(N_t) = \mathrm{k}t \tag{2}$$

where N_0 and N_t are the number of molecules at the initial time and any given time t, respectively. The rate constant is determined as the slope of the linear fit of $\ln(N_0) - \ln(N_t)$ versus time. The first-order rate law equation is used, since unimolecular reactions are found to be predominant during the high temperature pyrolysis of the fuels studied. The time required for 50% fuel consumption is used to calculate the rate constants in this work. Due to the low reactivity of 1,3-dioxolane, 50% fuel consumption is not achieved at 1800 K even during a relatively long simulation of 8 ns. Therefore, the rate constant for 1,3-dioxolane at 1800 K is calculated with the time required for 25% fuel consumption, same as in the previous ReaxFF studies [34,36].

Fig. 3 shows the logarithm of the rate constants obtained from ReaxFF at different temperatures against the inverse of temperature. It is observed that first-order kinetics fit well to the Arrhenius plot, with a coefficient of determination (R^2) of 0.996. The ReaxFF-derived rate constants are compared with experimentally measured rate constants for thermal decomposition of 1,3-dioxolane. Cutler *et al.* [10] and Guenther and Walters [9] measured the rate constants over 963–1093 K at 1 atm and 728–798 K at 0.07–0.5 atm, respectively, and determined the pre-

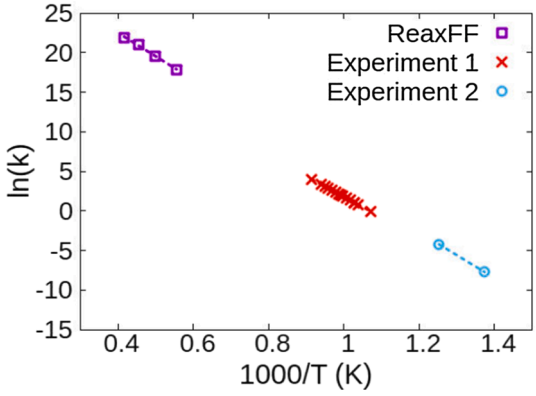


Fig 3. Logarithm of the global decomposition rate constant (k) plotted against the inverse of temperature (1000/T) for 1,3-dioxolane.

exponential factor (A) and activation energy (E_a). The experimentally determined Arrhenius parameters are listed in Table 1, together with those derived from ReaxFF simulations using the following Arrhenius equation,

$$k = A\exp(-E_a/RT) \quad (3)$$

where R is the ideal gas constant. As shown in Table 1, the activation energy calculated from ReaxFF is in good agreement with the experimental values. However, the predicted pre-exponential factor is a few orders of magnitude larger than the experimental data, which is the same trend observed in previous ReaxFF works [28,37,38]. The discrepancy probably occurs due to the high temperature and pressure conditions of the ReaxFF simulations compared to the experiment. Although the pre-exponential factor is often described as temperature independent over a small temperature range, it actually increases with temperature due to its dependence on frequency of collisions [39]. In addition, the pre-exponential factor may increase under the high pressure condition, because more molecules would have enough energy to react in a limited system [28]. Hence, considering the different operating conditions between ReaxFF and experiment, the pre-exponential factor calculated using the ReaxFF simulation lies within an acceptable range.

Next, we compare the ReaxFF-predicted product distribution with measurement. According to the literature [9,10], major products resulting from the pyrolysis of 1,3-dioxolane are H_2, CO, CO_2, CH_2O, CH_4, and C2 hydrocarbons. Fig. 4 shows the products with more than 2 % by mole fraction on average at the end of the ReaxFF simulations (2 ns for 2000 K – 2400 K and 8 ns for 1800 K), and the list of the major products is shown to be consistent with the measurements. C_2H_4O is only around 0.2 % at 2400 K by the end of the simulation, but it is included in Fig. 4 because it is a key intermediate species. At lower temperatures (2000 and 1800 K), CH_2O is the most abundant species, because it can be directly produced from 1,3-dioxolane by consecutive cleavages of the two C-O bonds or C-O bond and C–C bond. Although C_2H_4O is formed together with CH_2O, C_2H_4O has a much lower

Table 1
Fitted Arrhenius parameters for the global decomposition rates of 1,3-dioxolane and Fuels 1–3. Experiments 1 and 2 for 1,3-dioxolane are obtained from [10] and [9], respectively.

Compound	Method	E_a (kcal/mol)	A (1/s)
1,3-dioxolane	ReaxFF	58.8	8.3×10^{14}
	Experiment 1 [10]	44.8–57.8	$4.0 \times 10^{10} - 2.4 \times 10^{13}$
	Experiment 2 [9]	57.6	8.7×10^{13}
Fuel 1	ReaxFF	44.6	3.2×10^{14}
Fuel 2	ReaxFF	51.7	1.1×10^{15}
Fuel 3	ReaxFF	44.3	3.5×10^{14}

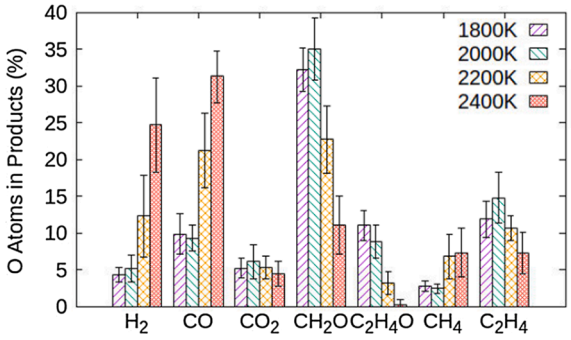


Fig 4. Major products from the thermal decomposition of 1,3-dioxolane. Products with more than 2 % by mole fraction on average at the end of the simulations (2 ns for 2000 K – 2400 K and 8 ns for 1800 K) are plotted. Statistical uncertainty ranges are specified based on ± 1 standard deviation from the averaged results of the 10 independent simulations.

concentration than CH_2O due to its faster consumption to CO and CH_4. With increasing temperature, the number of CO, H_2 and CH_4 molecules increases due to further decomposition of CH_2O and C_2H_4O. H_2 is primarily formed from H-abstraction reaction of CH_2O with H atom ($CH_2O + H \rightarrow CHO + H_2$). CHO and CH_3 produced from C_2H_4O are converted to CO and CH_4, respectively. For the generation of CO_2 and C_2H_4, there are two possible decomposition pathways. The first pathway occurs by direct decomposition of 1,3-dioxolane to CH_2O_2 and C_2H_4. CO_2 is formed by dehydrogenation reactions of CH_2O_2. The second pathway is initiated by H-abstraction of 1,3-dioxolane that produces $C_3H_5O_2$. Further decomposition of $C_3H_5O_2$ produces C_2H_4 and CHO_2, and CHO_2 eventually decomposes to CO_2. These reaction pathways extracted from ReaxFF simulations are consistent with previously proposed global decomposition pathways of 1,3-dioxolane based on the experimentally observed decomposition products [9,10]. Therefore, the results shown in Figs. 3 and 4 demonstrate that the ReaxFF employed in this study can be used to describe the pyrolysis of 1,3-dioxolane. Furthermore, for 4,5-dimethyl-2-methyl-1,3-dioxolane, which is common structure of Fuels 1–3, we additionally confirm that the ReaxFF reproduces reasonably well the molecular structure and bond dissociation energies (BDE) calculated using DFT method. Details on the DFT calculations and the BDE results are summarized in Section S2 of the supplemental material. These results demonstrate that the CHO-2016 force field can be used to predict the pyrolysis chemistry of the three alkyl-substituted dioxolanes selected in this work [8].

3.2. *Pyrolysis of alkyl-substituted 1,3-dioxolanes*

In this section, reaction rate constant and product spectrum during the pyrolysis of Fuels 1–3 (Fig. 1(b)-(d)) are investigated using ReaxFF simulations.

3.2.1. *Decomposition rate and reaction mechanism*

We investigate the thermal decomposition kinetics of the three alkyl-substituted 1,3-dioxolanes shown in Fig. 1. Fig. 5 shows the time evolution of the number of fuel molecules at temperatures ranging from 1800 K to 2400 K, with quantified statistical uncertainties. As expected, at higher temperatures, fuel molecules decompose faster for all three fuels. At a given temperature, Fuel 2 takes the longest time to be completely consumed, and the decomposition profiles of Fuel 1 and Fuel 3 are very similar. Following the procedure mentioned in the previous section, the decomposition rate constants are calculated for the three fuels at each temperature, as shown in Fig. 6, as a function of the inverse of temperature. The activation energy and pre-exponential factor, determined from the linear fit of this data (with $R^2 = 0.998$), are listed in Table 1. Fuel 2 has the highest pre-exponential factor (1.1×10^{15} 1/s) among the three dioxolane fuels, but shows the slowest decomposition

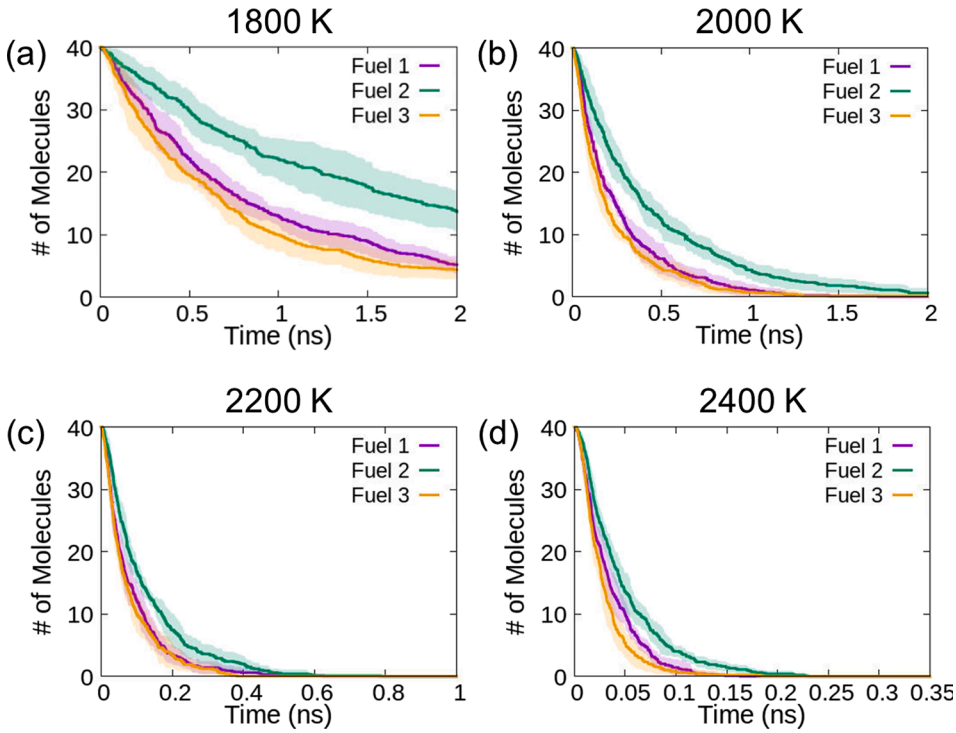


Fig 5. Time evolution of the number of fuel molecules at (a) 1800 K, (b) 2000 K, (c) 2200 K, and (d) 2400 K. The shaded regions indicate the statistical uncertainties estimated on the basis of ± 1 standard deviation from the averaged results of the 10 independent simulations.

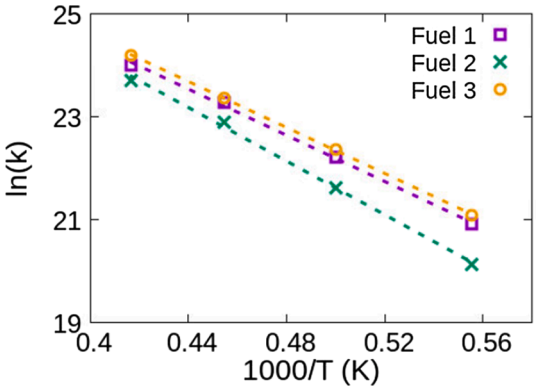
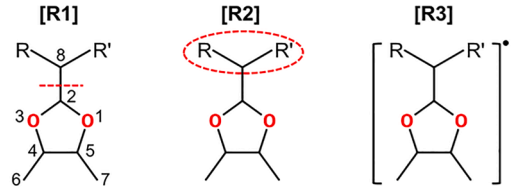


Fig 6. Logarithm of the global decomposition rate constant (k) plotted against the inverse of temperature (1000/T) for Fuels 1–3.

rate due to the highest activation energy (51.7 kcal/mol). Fuel 2 and Fuel 3 have very similar activation energy and pre-exponential factor. A key factor in determining the quality of diesel fuels is the cetane number, a measure of ignition delay. According to the literature, 1,3-dioxolane exhibits a relatively low cetane number of 30 [40]. On the other hand, the substituted 1,3-dioxolanes studied in this work have higher derived cetane numbers ranging from 44.8 to 64.2 [8]. The ReaxFF-derived Arrhenius parameters (Table 1) show that 1,3-dioxolane and the alkyl-substituted dioxolanes have comparable pre-exponential factors. However, the relatively high activation energy of 1,3-dioxolane results in its low reactivity (and consequently a poor cetane number), in qualitative agreement with previously determined cetane numbers for these fuels.

We also analyze the initial decomposition pathways for Fuels 1–3. Only the simulation results at 2000 K are discussed below as a representative case, since the initial decomposition pathways for all three fuels do not exhibit significant temperature-dependence. Results at other temperatures (1800 K, 2200 K, and 2400 K) are included in Section S3 of the supplementary material for completeness. Fig. 7 shows the



Fuel 1 (R = Et, R' = Et)	55.5 %	7.5 %	15.7 %	10.7 %	5.5 %
Fuel 2 (R = Bu, R' = H)	31.0 %	16.0 %	20.8 %	14.5 %	3.4 %
Fuel 3 (R = Bu, R' = Et)	55.9 %	10.5 %	16.3 %	8.3 %	3.0 %

Fig 7. Major initial decomposition reactions for Fuels 1–3 at 2000 K. R and R' denote Et (ethyl, C_2H_5), H (hydrogen atom, H), and Bu (butyl, C_4H_9) groups for different fuels.

important initial reactions and their relative contributions observed during the thermal decomposition of the three fuels. There are five main decomposition routes: (R1) C^2-C^8 bond scission between the alky side chain (R-C-R') and ring, (R2) C–C scission within the alkyl side-chain, (R3) H-abstraction, and (R4 and R5) ring-opening followed by C-O scission. The most preferred decomposition channel for the three alkyl-substituted dioxolane fuels is R1. About 56 % of Fuel 1 and Fuel 3 and 31 % of Fuel 2 are decomposed through R1. From this reaction, Fuel 1, Fuel 2, and Fuel 3 produce 3-pentyl (3-C_5H_{11}), 1-pentyl (1-C_5H_{11}), and 3-heptyl (3-C_7H_{15}), respectively, along with 4,5-dimethyl-1,3-dioxolane radical ($C_5H_9O_2$). R2 generates 1-alkyl radical and 4,5-dimethyl-1,3-dioxolane with a 1-alkene side-chain. The produced 4,5-dimethyl-1–3-dioxolane with a 1-alkene side-chain is primarily decomposed to 4,5-dimethyl-1,3-dioxolane radical and 1-alkene by C^2-C^8 bond scission (not shown in Fig. 7). H-abstraction reactions (R3) typically involve radicals, such as H and CH_3, and accounts for 15 – 21 % of the total fuel decomposition. R4 and R5 reactions occur by two consecutive C-O bond scissions. The first C-O bond scission opens the five-membered ring, and depending on the location of the second C-O bond scission, different products are formed. R4 by sequential bond scissions of C^4-O^3 and C^2-O^1 (or C^5-O^1 and C^2-O^3) generates two oxygenated species with one oxygen atom each. On the other hand, R5 by sequential bond scissions of C^4-O^3 and C^5-O^1 produces 2-C_4H_8 and oxygenated species with two oxygen atoms. As shown in Fig. 7, R5 (ring-opening 2) is less preferred than R4 (ring-opening 1). Overall, Fuel 1 and Fuel 3 show very similar initial decomposition routes, whereas the decomposition of Fuel 2 has higher contributions from R2, R3, and R4.

3.2.2. *Product distribution*

The initial reaction mechanism analysis presented above shows that the major initial decomposition products of the three alkyl-substituted 1,3-dioxolanes are 4,5-dimethyl-1,3-dioxolane radical and the hydrocarbons derived from the R-C-R' side-chain (via R1), as shown in Fig. 8. The subsequent reactions of these initial products can be broadly divided into two parts: decomposition of (1) 4,5-dimethyl-1,3-dioxolane radical and (2) R-C-R' side-chain. As presented in Figs. 8, 4,5-dimethyl-1,3-dioxolane radical produced from the decomposition of all three fuels is decomposed by two consecutive C-O bond scissions forming 2-butene (2-C_4H_8) and formate (HCO_2). The relatively unstable HCO_2 radical is converted into a stable species, CO_2, by losing H atom.

The R-C-R' side-chain breaks down to alkyl radial and alkene by C–C bond cleavage during high-temperature pyrolysis. The produced alkyl radical further decomposes to smaller alkyl and alkene species by C–C bond cleavage. Therefore, alkenes are the major stable hydrocarbon products of the three alkyl-substituted 1,3-dioxolane fuels studied in this work. Fig. 9 shows the time evolution of ethylene (C_2H_4), propene (C_3H_6), and butene (C_4H_8) during the pyrolysis simulations at 2000 K. Note that all butene isomers are lumped in C_4H_8 in the plots. The distribution of the alkene products is largely affected by the structure of the alkyl side-chain (R-C-R'). Fuels 1 and 2 have 3-C_5H_{11} and 1-C_5H_{11} side-chains, respectively, and the decomposition of the two pentyl isomers leads to quite different products. Although these two fuels produce a similar amount of C_3H_6, Fuel 1 tends to produce more C_4H_8 and less C_2H_4 than Fuel 2 (Fig. 9). 3-C_5H_{11} produced from Fuel 1 preferentially decomposes to C_3H_6 + C_2H_5 and C_4H_8 + CH_3, and C_2H_5 further decomposes to C_2H_4 (Fig. 10a). On the other hand, C_4H_8 formation is not preferred in the decomposition of 1-C_5H_{11} produced from Fuel 2. Instead, 1-C_5H_{11} dominantly breaks down to C_2H_4 + C_3H_7 and C_3H_6 + C_2H_5 (Fig. 10b). The alkyl radicals, such as C_3H_7 and C_2H_5, further decompose to C_2H_4. Fuel 3, which has a 3-C_7H_{15} side-chain, produces the highest amount of C_4H_8 (Fig. 9c) with an amount of C_2H_4 comparable to Fuel 2. The most preferred initial products of 3-C_7H_{15} are C_4H_8 + C_3H_7, and consecutively C_3H_7 breaks down to C_2H_4 + CH_3 (Fig. 10c). Other minor pathways produce C_3H_6 + C_4H_9, C_5H_{10} + C_2H_5, and C_6H_{12} + CH_3 with similar contributions (11 – 13 %), as shown in Fig. 10.

Staples *et al.* [8] measured the sooting tendencies of the three alkyl-substituted 1,3-dioxolanes using the well-established soot propensity quantification metric, Yield Sooting Index (YSI) [41–43]. The measured YSIs of Fuel 1, Fuel 2, and Fuel 3 are 58, 49, and 69, respectively. This indicates that the sooting tendency increases in the following order, Fuel 2 < Fuel 1 < Fuel 3. The distribution of C2-C4 alkene products identified using ReaxFF in Fig. 9 can be used to qualitatively explain the measured YSI trend, similar to previous ReaxFF-based studies [34,44]. It is generally known that a larger alkene is a more effective precursor in the formation of the first aromatic ring (*e.g.* benzene), which is a key step towards the formation of polycyclic aromatic hydrocarbons (PAHs) and ultimately soot [45]. Specifically, C_2H_4 is a less effective non-aromatic soot precursor than C_3H_6, since it requires slow addition reactions to produce C3 radicals, such as C_3H_3 and C_3H_5, that are essential precursors for benzene formation [46,47]. On the other hand, C_4H_8 can produce the key C3 radicals more rapidly by C–C fission than C_3H_6. Therefore, C_4H_8 is a more effective non-aromatic soot precursor than C_3H_6. Fig. 9 shows that the three alkyl-substituted 1,3-dioxolanes generate a similar amount of C_3H_6, with different levels of C_2H_4 and C_4H_8. Fuel 1 produces less C_2H_4 but more C_4H_8 than Fuel 2. This suggests that Fuel 1 has a higher sooting tendency than Fuel 2, since C_4H_8 is a more effective precursor than C_2H_4 for the formation of the first aromatic ring. Fuel 3 produces more C_4H_8 and C_2H_4 than Fuel 1, which suggests that it has the highest sooting tendency among the three fuels. These ReaxFF predictions are consistent with the trends in previously reported YSI measurements [8].

Oxygenated products containing the oxygen atoms initially present in the three alkyl-substituted 1,3-dioxolanes (2 per fuel molecule) are further analyzed. Fig. 11 shows the distribution of oxygenated compounds at the end of the simulations (2 ns). 69 %, 64 %, and 75 % of the total oxygen atoms end in the form of CO_2 for Fuel 1, Fuel 2, and Fuel 3, respectively. As shown in Fig. 8, this is caused by the preferential production of CO_2 from the 4,5-dimethyl-1,3-dioxolane radical. In addition,

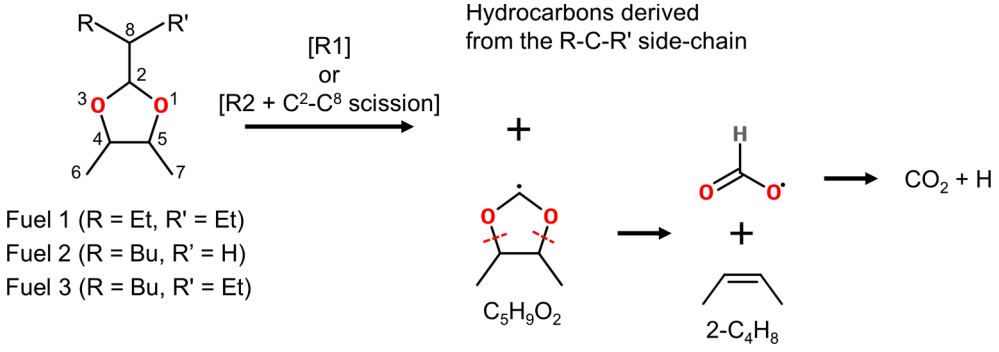


Fig 8. Major decomposition pathways of the three alkyl-substituted 1,3-dioxolanes. R and R' denote Et (ethyl, C_2H_5), H (hydrogen atom, H), and Bu (butyl, C_4H_9) groups for different fuels.

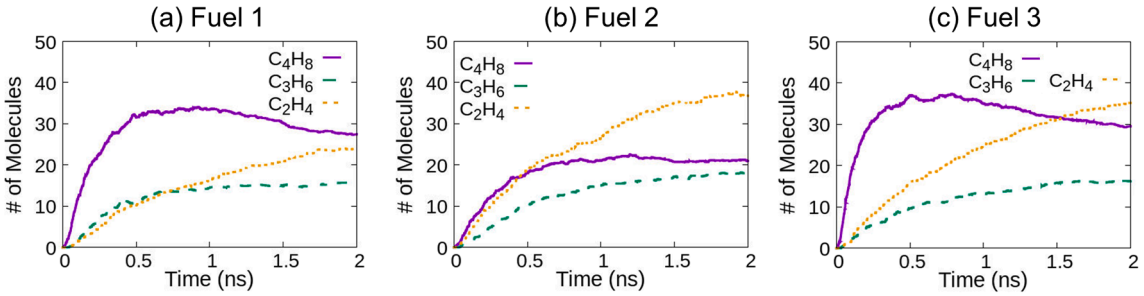


Fig 9. Time evolution of C_2H_4, C_3H_6, and C_4H_8 (all butene isomers lumped together) during the pyrolysis simulations of Fuels 1–3 at 2000 K.

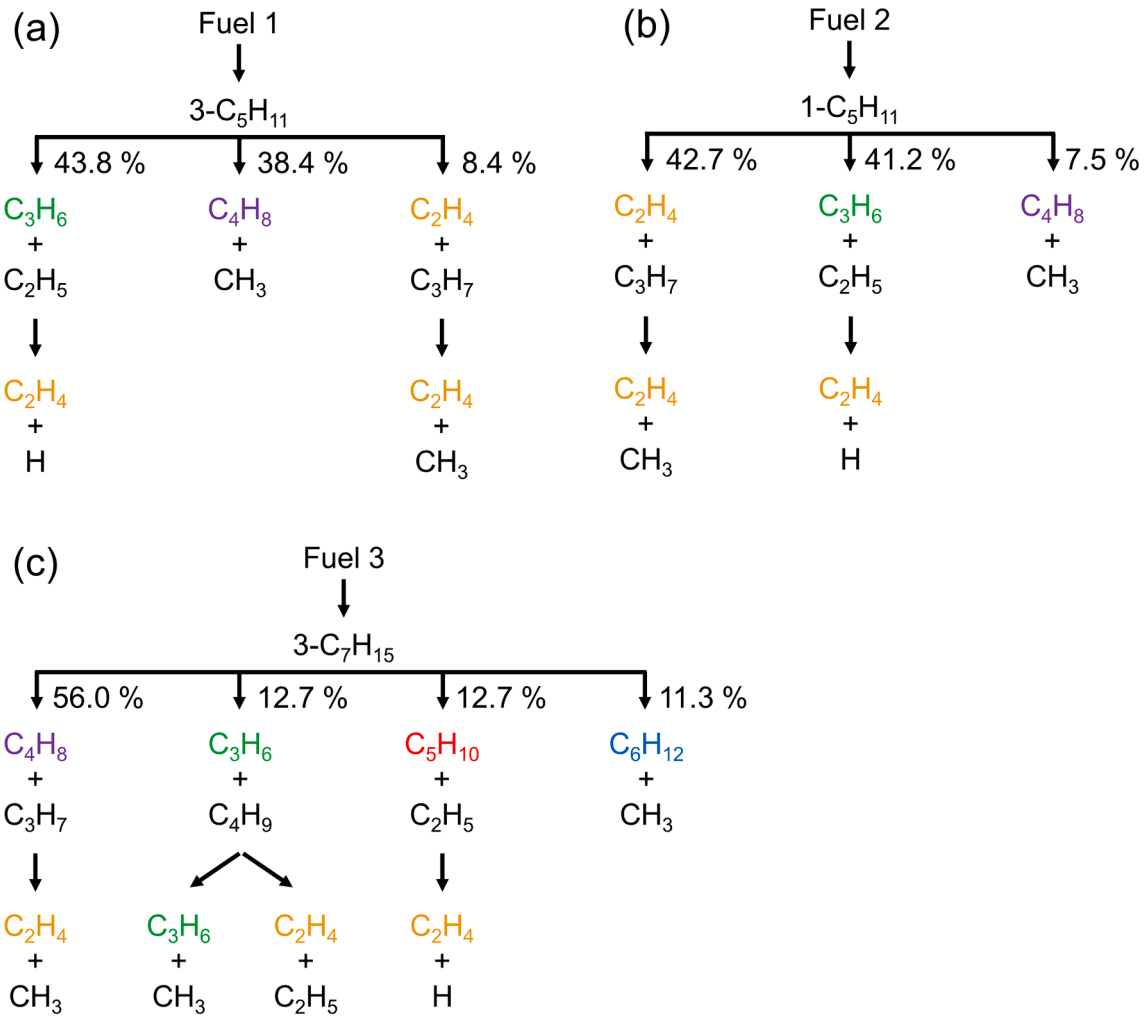


Fig 10. Decomposition of the alkyl side-chains of the three alkyl-substituted 1,3-dioxolanes at 2000 K. The black and colored fonts indicate radicals and alkenes, respectively.

reactions initiated by R5 eventually can contribute to the production of CO_2, even though it only accounts for a small part of the total decomposition (<5.5 %). The second preferred oxygenated product is CO. One possible route to form CO is through R4 that generates two oxygenated species. Since each of the two oxygenated species have one oxygen atom, CO can be eventually produced from R4-initiated reactions. The CO production pathways are summarized in Section S4 of the supplementary material. If the simulation time is longer, more CO is expected to form since CH_2O will likely be converted to CO by losing H atoms. However, CO production is much less than CO_2 even after considering the CH_2O to CO pathway. As shown earlier, the alkyl-substituted 1,3-dioxolane fuels are mostly decomposed by unimolecular bond scissions, therefore, the formation of H_2O is not significant (<4 % in Fig. 11). The rest of the oxygen-containing species are lumped in "Others" in Fig. 11, which contain only 6–10 % of the total oxygen atoms. The further decomposition of these compounds will likely not change the main conclusion that CO_2 is the most preferred oxygen-containing product of the three alkyl-substituted 1,3-dioxolane fuels.

3.3. *A strategy to potentially reduce soot yield from dioxolane fuels*

It is well-known that oxygenated hydrocarbons can have smaller sooting tendencies than the corresponding hydrocarbons with similar molecular structure, because the carbon atoms bonded with oxygen

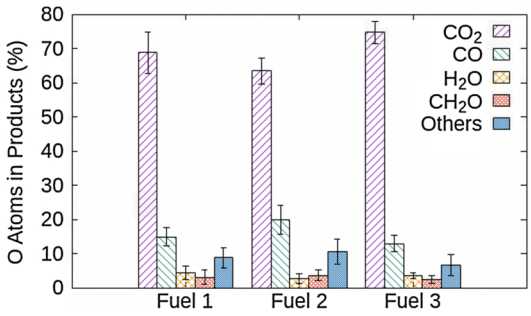


Fig 11. Distribution of oxygen-containing compounds at the end of the pyrolysis simulations for Fuels 1–3 (2 ns) at 2000 K. Statistical uncertainty ranges are specified based on ± 1 standard deviation from the averaged results of the 10 independent simulations.

atoms do not contributed to soot formation [48,49]. The effectiveness of an oxygen atom in soot reduction depends largely on how many carbon atoms are bonded to it. In the ideal case, one carbon atom can be removed from potentially producing soot by one oxygen atom. From this point of view, the oxygen atoms in the three alkyl-substituted dioxolanes considered in this work do not optimally contribute to soot reduction. As shown in Fig. 11, a significant number of oxygen atoms tend to bind a half of carbon per oxygen rather than one carbon by dominantly producing CO_2.

In this section, we propose a strategy to control the oxygen flux during the pyrolysis of alkyl-substituted 1,3-dioxolane fuels by changing the molecular structure and keeping the same carbon number, which could potentially further reduce soot formation. We discussed in Section 3.2.1 that the dioxolane ring breaking involves two C-O bond cleavages, and different products are generated depending on the location of the C-O bonds broken. Reaction route R5 (Ring-opening 2 in Fig. 7) by C^4-O^3 and C^5-O^1 scissions produces a hydrocarbon fragment and another compound containing two oxygens, and CO_2 is likely to be produced eventually from the latter. On the other hand, Reaction route R4 (Ring-opening 1 in Fig. 7) by C^4-O^3 and C^2-O^1 scissions (or C^5-O^1 and C^2-O^3 scissions) produces two oxygenated species, each with one oxygen atom. These two oxygenated products would potentially decompose to two C1 species containing one oxygen atom, such as CO and CH_2O, which is the desired scenario for soot reduction (one carbon is combined with one oxygen). However, as shown in Figs. 7 and 8, all three alkyl-substituted 1,3-dioxolanes studied in this work produce 4,5-dimethyl-1,3-dioxolane radical as the major oxygenated intermediate, which eventually generates CO_2 by Reaction route R5 (Ring-opening 2). Hence, our strategy is to move the side-chain (R-C-R') from its current position to connect it with C^6 or C^7 so that the formation of 4,5-dimethyl-1,3-dioxolane radical is suppressed. As such, we expect that the modified dioxolanes to decompose more by Ring-opening 1 than Ring-opening 2, thereby increasing the effectiveness of the oxygen atoms in soot reduction. To validate our strategy, we designed a new dioxolane fuel, Fuel 4 (4-hexyl-5-methyl-1,3-dioxolane; $C_{10}H_{20}O_2$), by rearranging the side chain location of Fuel 2, as illustrated in Fig. 12.

The pyrolysis of Fuel 4 is simulated under the exact same conditions as Fuels 1–3, and all the results shown for Fuel 4 are averaged from 10 independent simulations. Fig. 13a shows the time evolution of the number of Fuel 2 and Fuel 4 molecules at 2000 K. Fuel 4 shows a slightly slower decomposition rate than Fuel 2 until approximately 0.75 ns. Thereafter, the decomposition rates of the two fuels are almost the same. This result indicates that the reactivity and other reactivity-related properties (*e.g.*, ignition) of the new fuel (Fuel 4) are comparable to Fuel 2. Fig. 13b compares the time evolution of the number of C2-C4 alkenes formed from Fuel 4 and Fuel 2 decomposition. Fuel 4 and Fuel 2 generate a similar level of C_3H_6 and C_2H_4 at all simulation times. However, Fuel 4 produces much less C_4H_8 than Fuel 2. In Fuel 2 decomposition, as shown in Fig. 8, the most preferable C_4H_8 formation route is through ring-opening 2 of 4,5-dimethyl-1,3-dioxolane radical. However, this route is no longer preferred in Fuel 4 decomposition. Instead, the initial decomposition of Fuel 4 primarily happens by the decomposition route R5 (Ring-opening 2 in Fig. 7), as shown in Fig. 15. Therefore, the formation of C_4H_8, an effective non-aromatic soot precursor, is noticeably reduced in Fuel 4 pyrolysis, which potentially can lead to soot reduction.

Fig. 14 compares the distribution of oxygen-containing compounds at the end of the pyrolysis simulations (2 ns) for Fuel 2 and Fuel 4 at 2000 K. As expected, Fuel 4 produces CO more preferentially than CO_2 compared to Fuel 2. 63.5% of the total oxygen atoms are contained in CO_2 for Fuel 2, whereas only 11.2 % of the oxygen atoms are in CO_2 for Fuel 4. On the other hand, the fraction of oxygen atoms contained in CO molecules increases from 19.8 % (Fuel 2) to 33.5 % (Fuel 4). In addition, for Fuel 4, 34 % of oxygen atoms end in CH_2O, which would likely be further converted to CO, if the simulation time is longer. These results suggest that the molecular structure of Fuel 4, modified based on Fuel 2 by keeping the same carbon number, allows for the oxygen atoms to more effectively take away carbon atoms that can potentially form soot.

To identify the CO formation pathways during Fuel 4 pyrolysis, we also performed the reaction pathway analysis, as shown in Fig. 15. It is found that the decomposition route R5 (Ring-opening 2 in Fig. 7), which is a major initial decomposition reaction for Fuel 2 leading to CO_2 production, is indeed suppressed in Fuel 4 pyrolysis. Instead, initial reaction of Fuel 4 primarily occurs by the decomposition route R4 (Ring-opening 1 in Fig. 7), C–C scission, and H-abstraction from the alkyl chain. Each decomposition route goes through several steps and eventually produces two CO molecules. On the other hand, the major CO_2 formation pathways in Fuel 4 decomposition are shown to be R5 (Ring-opening 2), followed by dehydrogenation of CH_2O_2 to CO_2. In addition, reactions initiated by H-abstraction can also contribute to the production of CO_2. These CO_2 production pathways for Fuel 4 are summarized in Section S5 of the supplemental material. These results confirm that Fuel 4 preferentially produces CO over CO_2, which can potentially help reduce soot yield. Note that this suggested molecular design (Fuel 4) is entirely based on ReaxFF simulation predictions, and experimental measurements would be required to fully validate the conclusions reported here. However, this is beyond the scope of the current work.

4. Conclusions

The main purpose of this work was to study the pyrolysis of three

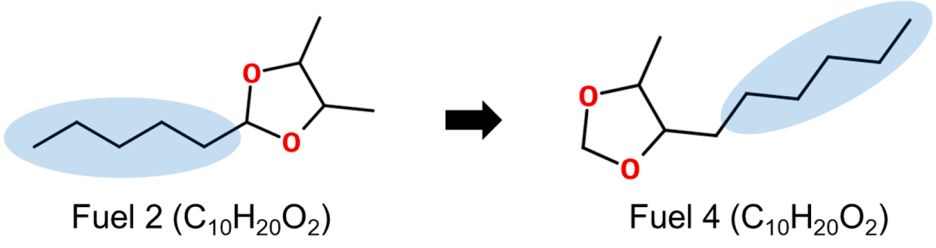


Fig 12. Molecular structure of Fuel 4 (4-hexyl-5-methyl-1,3-dioxolane), modified based on Fuel 2.

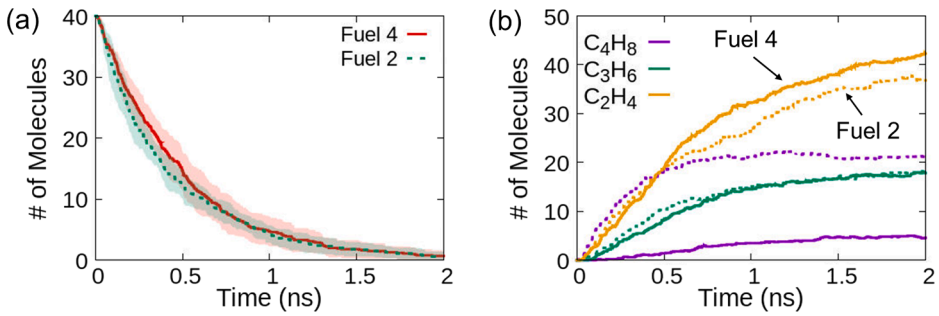


Fig 13. Comparison of the pyrolysis behaviors of Fuel 4 and Fuel 2 at 2000 K. (a) Time evolution of the number of (a) fuel molecules and (b) major alkene products. In (b), solid and dotted lines indicate the compounds produced from Fuel 4 and Fuel 2, respectively. The Fuel 2 data are extracted from Fig. 5b and 9b for comparison.

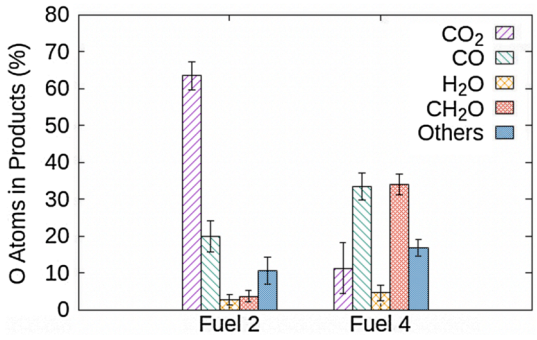


Fig 14. Distribution of oxygen-containing compounds at the end of the pyrolysis simulations for Fuel 2 and Fuel 4 (2 ns) at 2000 K. The data for Fuel 2 is extracted from Fig. 11 and added for comparison. Statistical uncertainty ranges are specified based on ± 1 standard deviation from the averaged results of the 10 independent simulations.

alkyl-substituted 1,3-dioxolanes (Fuels 1–3 shown in Fig. 1) at high-temperatures (1800 K – 2400 K) using ReaxFF-MD simulations. For the three alkyl-substituted 1,3-dioxolanes considered in this work, the decomposition rate, reaction mechanism, and product distribution were analyzed. The three fuels primarily decomposed to 4,5-dimethyl-1,3-dioxolane radical and hydrocarbons derived from the R-C-R' side-chain. 4,5-dimethyl-1,3-dioxolane radical was further decomposed and eventually produced 2-C_4H_8 and CO_2. Depending on the molecular structure of the R-C-R' side-chain, the product distribution (C2-C4 alkenes) significantly varied, and this had a strong influence on the sooting tendency of these fuels. Based on the amount of C2-C4 alkenes produced, ReaxFF predicted that the order of sooting tendency was Fuel 3 > Fuel 1 > Fuel 2, which is in agreement with the experimentally measured YSI trend.

We proposed a new alkyl-substituted 1,3-dioxolane fuel (Fuel 4, 4-hexyl-5-methyl-1,3-dioxolane), which might produce less soot, by modifying the molecular structure of Fuel 2 and keeping the same carbon number. Fuel 4 was shown to produce much less C_4H_8, an effective non-aromatic soot precursor, compared to Fuel 2. CO_2 was produced more favorably by Fuel 2, whereas CO was produced preferentially by

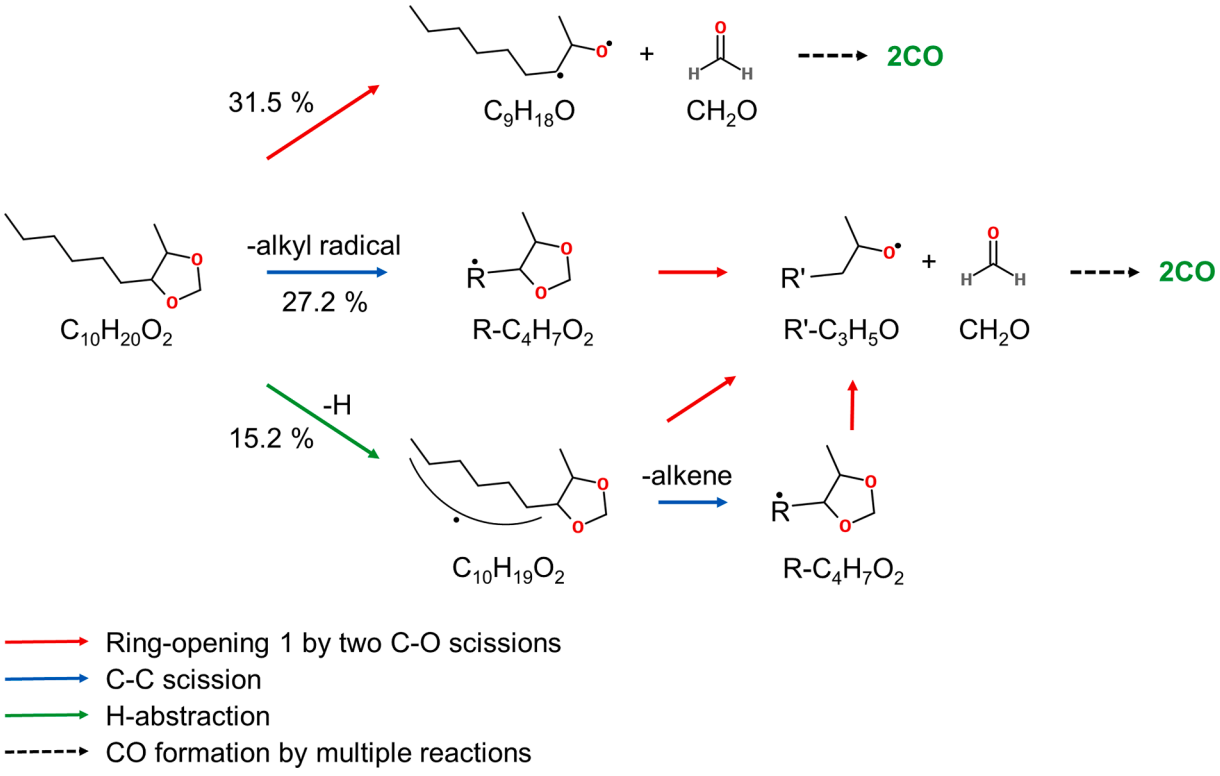


Fig 15. Major CO formation pathways during Fuel 4 pyrolysis.

Fuel 4. The preferred production of CO over CO_2 would help reduce soot yield by removing more carbon atoms from the soot-producing pool of hydrocarbons per oxygen atom.

The reaction pathways identified in this work can be used to develop chemical kinetic models for 1,3-dioxolane based biodiesel compounds, applicable to combustion engine simulations, with much lower computational cost compared to density function theory-based calculations. This work also demonstrated that the chemical kinetic information from ReaxFF simulations can help design new fuels with more desired properties.

CRediT authorship contribution statement

Hyunguk Kwon: Conceptualization, Formal analysis, Investigation, Writing - original draft, Writing - review & editing. **Yuan Xuan:** Conceptualization, Writing - review & editing, Resources, Supervision, Project administration, Funding acquisition.

Declaration of Competing Interest

The authors declare that they have no known competing financial interests or personal relationships that could have appeared to influence the work reported in this paper.

Acknowledgments

This research was funded by the U.S. Department of Energy's Office of Energy Efficiency and Renewable Energy (EERE) under the Bioenergy Technologies Office (BETO) and Vehicle Technologies Office (VTO) Program Award Number DE-EE0007983.

References

[1] Huber GW, Iborra S, Corma A. Synthesis of transportation fuels from biomass: chemistry, catalysts, and engineering. Chem Rev 2006;106(9):4044–98.
[2] Climent MJ, Corma A, Iborra S. Conversion of biomass platform molecules into fuel additives and liquid hydrocarbon fuels. Green Chem 2014;16(2):516–47.
[3] Kohse-Höinghaus K, Oßwald P, Cool T, Kasper T, Hansen N, Qi F, et al. Biofuel combustion chemistry: From ethanol to biodiesel. Angew Chem Int Ed 2010;49 (21):3572–97.
[4] Ribeiro NM, Pinto AC, Quintella CM, da Rocha GO, Teixeira LSG, Guarieiro LLN, et al. The Role of Additives for Diesel and Diesel Blended (Ethanol or Biodiesel) Fuels: A Review. Energy Fuels 2007;21(4):2433–45.
[5] Oh Y-K, Hwang K-R, Kim C, Kim JR, Lee J-S. Recent developments and key barriers to advanced biofuels: A short review. Bioresour Technol 2018;257:320–33.
[6] Harvey BG, Merriman WW, Quintana RL. Renewable Gasoline, Solvents, and Fuel Additives from 2,3-Butanediol. ChemSusChem 2016;9(14):1814–9.
[7] Harrison KW, Harvey BG. High cetane renewable diesel fuels prepared from bio-based methyl ketones and diols. Sustainable Energy Fuels 2018;2(2):367–71.
[8] Staples O, Moore C, Leal JH, Semelsberger TA, McEnally CS, Pfefferle LD, et al. A simple, solvent free method for transforming bio-derived aldehydes into cyclic acetals for renewable diesel fuels. Sustainable Energy Fuels 2018;2(12):2742–6.
[9] Guenther WB, Walters WD. The thermal decomposition of dioxolane. J Am Chem Soc 1951;73(5):2127–31.
[10] Cutler AH, Antal MJ, Jones M. Kinetics and mechanism of the vapor phase pyrolysis of 1,3-dioxolane in steam. J Anal Appl Pyrolysis 1987;12(3-4):223–42.
[11] Roquitte BC. The Photochemistry of 1,3-Dioxolane. J Phys Chem 1966;70(9): 2863–8.
[12] Çetinkaya E, Schuchmann H-P, von Sonntag C. Radiation chemistry of acetals. Part 4. Photolysis (λ 185) of liquid 1,3-dioxolan and 2,2-dimethyl-1,3-dioxolan. J Chem Soc, Perkin Trans 2 1978;(10):985–9. https://doi.org/10.1039/P29780000985.
[13] Mel'nikov MY, Baskakov DV, Mel'nikova OL, Feldman VI. Photochemistry of 1,3-dioxolane radical cations in sulfur hexafluoride and freonic matrices at 77 K. High Energ Chem 2002;36(2):103–11.
[14] Fernández-Sánchez E, García-Domínguez JA, De la Iglesia-Gayá B. Radical-sensitized thermal decomposition of 1,3-dioxolane in the gas phase. J Anal Appl Pyrolysis 1991;18(3-4):219–32.
[15] Sauer CG, Barnes I, Becker KH, Geiger H, Wallington TJ, Christensen LK, et al. Atmospheric Chemistry of 1,3-Dioxolane: Kinetic, mechanistic, and modeling study of OH radical initiated oxidation. J Phys Chem A 1999;103(30):5959–66.
[16] Freitas Dinis CM, Geiger H, Wiesen P. Kinetics of the reactions of OH(X2Π) radicals with 1,3-dioxolane and selected dialkoxy methanes. Phys Chem Chem Phys 2001;3 (14):2831–5.
[17] Le Calvé S, Mellouki A, Le Bras G. Kinetic studies of OH reactions with propylal, butylal and 1,3-dioxolane. Phys Chem Chem Phys 2002;4(22):5622–6.
[18] Rosas F, Lezama J, Mora JR, Maldonado A, Cordova T, Chuchani G. Kinetics and Mechanisms of the Thermal Decomposition of 2-Methyl-1,3-dioxolane, 2,2-Dimethyl-1,3-dioxolane, and Cyclopentanone Ethylene Ketal in the Gas Phase. Combined Experimental and DFT Study. J Phys Chem A 2012;116(37):9228–37.
[19] van Duin ACT, Dasgupta S, Lorant F, Goddard WA. ReaxFF: A reactive force field for hydrocarbons. J Phys Chem A 2001;105(41):9396–409.
[20] Chenoweth K, van Duin ACT, Goddard WA. ReaxFF reactive force field for molecular dynamics simulations of hydrocarbon oxidation. J Phys Chem A 2008; 112(5):1040–53.
[21] Senftle TP, Hong S, Islam MM, Kylasa SB, Zheng Y, Shin YK, et al. The ReaxFF reactive force-field: development, applications and future directions. Npj Comput Mater 2016;2(1). https://doi.org/10.1038/npjcompumats.2015.11.
[22] Mortier WJ, Ghosh SK, Shankar S. Electronegativity-equalization method for the calculation of atomic charges in molecules. J Am Chem Soc 1986;108(15): 4315–20.
[23] te Velde G, Bickelhaupt FM, Baerends EJ, Fonseca Guerra C, van Gisbergen SJA, Snijders JG, et al. Chemistry with ADF. J Comput Chem 2001;22(9):931–67.
[24] Castro-Marcano F, van Duin ACT. Comparison of thermal and catalytic cracking of 1-heptene from ReaxFF reactive molecular dynamics simulations. Combust Flame 2013;160(4):766–75.
[25] Wang Q-D, Wang J-B, Li J-Q, Tan N-X, Li X-Y. Reactive molecular dynamics simulation and chemical kinetic modeling of pyrolysis and combustion of n-dodecane. Combust Flame 2011;158(2):217–26.
[26] Cheng X-M, Wang Q-D, Li J-Q, Wang J-B, Li X-Y. ReaxFF molecular dynamics simulations of oxidation of toluene at high temperatures. J Phys Chem A 2012;116 (40):9811–8.
[27] Liu L, Bai C, Sun H, Goddard WA. Mechanism and Kinetics for the Initial Steps of Pyrolysis and Combustion of 1,6-Dicyclopropane-2,4-hexyne from ReaxFF Reactive Dynamics. J Phys Chem A 2011;115(19):4941–50.
[28] Ashraf C, van Duin ACT. Extension of the ReaxFF combustion force field toward syngas combustion and initial oxidation kinetics. J Phys Chem A 2017;121(5): 1051–68.
[29] Arvelos S, Abrahão O, Eponina Hori C. ReaxFF molecular dynamics study on the pyrolysis process of cyclohexanone. J Anal Appl Pyrolysis 2019;141:104620. https://doi.org/10.1016/j.jaap.2019.05.009.
[30] Kwon H, Shabnam S, van Duin ACT, Xuan Y. Numerical simulations of yield-based sooting tendencies of aromatic fuels using ReaxFF molecular dynamics. Fuel 2019; 262(15):116545.
[31] Ashraf C, Shabnam S, Jain A, Xuan Y, van Duin ACT. Pyrolysis of binary fuel mixtures at supercritical conditions: A ReaxFF molecular dynamics study. Fuel 2019;235:194–207.
[32] Chen Z, Sun W, Zhao L. Combustion mechanisms and kinetics of fuel additives: A ReaxFF molecular simulation. Energy Fuels 2018;32(11):11852–63.
[33] Chen Z, Sun W, Zhao L. Initial mechanism and kinetics of diesel incomplete combustion: ReaxFF molecular dynamics based on a multicomponent fuel model. The Journal of Physical Chemistry C 2019;123(14):8512–21.
[34] Kwon H, Lele A, Zhu J, McEnally CS, Pfefferle LD, Xuan Y, et al. ReaxFF-based molecular dynamics study of bio-derived polycyclic alkanes as potential alternative jet fuels. Fuel 2020;279:118548. https://doi.org/10.1016/j.fuel.2020.118548.
[35] Berendsen HJC, Postma JPM, van Gunsteren WF, DiNola A, Haak JR. Molecular dynamics with coupling to an external bath. J Chem Phys 1984;81(8):3684–90.
[36] Lele A, Kwon H, Ganeshan K, Xuan Y, van Duin ACT. ReaxFF molecular dynamics study on pyrolysis of bicyclic compounds for aviation fuel. Fuel 2021;297:120724. https://doi.org/10.1016/j.fuel.2021.120724.
[37] Chen T, Ku X, Li T, Karlsson BSA, Sjöblom J, Ström H. High-temperature pyrolysis modeling of a thermally thick biomass particle based on an MD-derived tar cracking model. Chem Eng J 2020:127923.
[38] Chenoweth K, van Duin ACT, Dasgupta S, Goddard III WA. Initiation mechanisms and kinetics of pyrolysis and combustion of JP-10 hydrocarbon jet fuel. J Phys Chem A 2009;113(9):1740–6.
[39] Criado JM, Pérez-Maqueda LA, Sánchez-Jiménez PE. Dependence of the preexponential factor on temperature. J Therm Anal Calorim 2005;82(3):671–5.
[40] Song J, Zello V, Boehman AL, Waller FJ. Comparison of the Impact of Intake Oxygen Enrichment and Fuel Oxygenation on Diesel Combustion and Emissions. Energy Fuels 2004;18(5):1282–90.
[41] McEnally CS, Das DD, Pfefferle LD. Yield sooting index database volume 2: Sooting tendencies of a wide range of fuel compounds on a unified scale. Harvard Dataverse V1 2017..
[42] Das DD, St. John PC, McEnally CS, Kim S, Pfefferle LD. Measuring and predicting sooting tendencies of oxygenates, alkanes, alkenes, cycloalkanes, and aromatics on a unified scale. Combust Flame 2018;190:349–64.
[43] Kwon H, Lapointe S, Zhang K, Wagnon SW, Pitz WJ, Zhu J, et al. Sooting tendencies of 20 bio-derived fuels for advanced spark-ignition engines. Fuel 2020; 276:118059. https://doi.org/10.1016/j.fuel.2020.118059.
[44] Kwon H, Etz BD, Montgomery MJ, Messerly R, Shabnam S, Vyas S, et al. Reactive molecular dynamics simulations and quantum chemistry calculations to investigate soot-relevant reaction pathways for hexylamine isomers. J Phys Chem A 2020;124 (21):4290–304.
[45] McEnally CS, Pfefferle LD, Atakan B, Kohse-Höinghaus K. Studies of aromatic hydrocarbon formation mechanisms in flames: Progress towards closing the fuel gap. Prog Energy Combust Sci 2006;32(3):247–94.
[46] McEnally CS, Pfefferle LD. Fuel decomposition and hydrocarbon growth processes for oxygenated hydrocarbons: butyl alcohols. Proc Combust Inst 2005;30(1): 1363–70.

[47] Jin H, Wang G, Wang Y, Zhang X, Li Y, Zhou Z, et al. Experimental and kinetic modeling study of laminar coflow diffusion methane flames doped with iso-butanol. Proc Combust Inst 2017;36(1):1259–67.

[48] Westbrook CK, Pitz WJ, Curran HJ. Chemical kinetic modeling study of the effects of oxygenated hydrocarbons on soot emissions from diesel engines. J Phys Chem A 2006;110(21):6912–22.

[49] McEnally CS, Pfefferle LD. Sooting tendencies of oxygenated hydrocarbons in laboratory-scale flames. Environ Sci Technol 2011;45(6):2498–503.